Sodium-Ion Batteries

Deutsche Ausgabe: DOI: 10.1002/ange.201602202
Internationale Ausgabe: DOI: 10.1002/anie.201602202

Suppressing the P2–O2 Phase Transition of $Na_{0.67}Mn_{0.67}Ni_{0.33}O_2$ by Magnesium Substitution for Improved Sodium-Ion Batteries

Peng-Fei Wang, Ya You, Ya-Xia Yin, Yue-Sheng Wang, Li-Jun Wan, Lin Gu, and Yu-Guo Guo**

Abstract: *Room-temperature sodium-ion batteries (SIBs) have shown great promise in grid-scale energy storage, portable electronics, and electric vehicles because of the abundance of low-cost sodium. Sodium-based layered oxides with a P2-type layered framework have been considered as one of the most promising cathode materials for SIBs. However, they suffer from the undesired P2–O2 phase transition, which leads to rapid capacity decay and limited reversible capacities. Herein, we show that this problem can be significantly mitigated by substituting some of the nickel ions with magnesium to obtain $Na_{0.67}Mn_{0.67}Ni_{0.33-x}Mg_xO_2$ ($0 \le x \le 0.33$). Both the reversible capacity and the capacity retention of the P2-type cathode material were remarkably improved as the P2–O2 phase transition was thus suppressed during cycling. This strategy might also be applicable to the modulation of the physical and chemical properties of layered oxides and provides new insight into the rational design of high-capacity and highly stable cathode materials for SIBs.*

The use of renewable electricity to address the global energy demand requires effective means for electric-energy storage. Although lithium-ion batteries offer the highest energy density among all secondary batteries, concerns regarding the lithium availability and its rising cost have driven researchers to investigate sustainable alternatives for energy storage.[1] Therefore, sodium-ion batteries (SIBs) have made a major comeback because of the natural abundance of sodium and the wide distribution of sodium resources.[1] New cathode materials for SIB systems are thus indispensable. A broad range of compounds, including oxides,[2] polyanionic frameworks,[3] and hexacyanoferrates,[4] have been studied as possible cathode materials, and layered oxides were found to be promising candidates as high-capacity cathode materials for SIBs.

[*] P.-F. Wang, Y. You, Dr. Y.-X. Yin, Prof. L.-J. Wan, Prof. Y.-G. Guo
CAS Key Laboratory of Molecular Nanostructure and Nanotechnology, Beijing National Laboratory for Molecular Sciences
Institute of Chemistry, Chinese Academy of Sciences (CAS)
Beijing 100190 (P.R. China)
E-mail: ygguo@iccas.ac.cn
P.-F. Wang, Prof. Y.-G. Guo
University of Chinese Academy of Sciences
Beijing 100049 (P.R. China)
Y.-S. Wang, Prof. L. Gu
Beijing National Laboratory for Condensed Matter Physics
Institute of Physics, Chinese Academy of Sciences (CAS)
Beijing 100190 (P.R. China)
E-mail: l.gu@iphy.ac.cn

Supporting information for this article can be found under: http://dx.doi.org/10.1002/anie.201602202.

Following the successful development of lithium ion insertion materials, sodium-based layered oxides, Na_xTMO_2 (TM = transition metal, e.g., Co, Fe, Mn, Ni, V; these can be grouped into two families, namely P2-type and O3-type structures), have been extensively investigated as model cathode materials for SIBs since the early 1980s.[5] Compared with O3-type Na_xTMO_2 materials, such as Na_xCoO_2,[6] Na_xMnO_2,[7] and $Na_xNi_{0.5}Mn_{0.5}O_2$,[8] P2-type mixed-transition-metal layered frameworks, such as $Na_{0.5}[Ni_{0.23}Fe_{0.13}Mn_{0.63}]O_2$,[9] have open prismatic paths for sodium diffusion with a low Na ion diffusion barrier, which makes the P2 phase a promising cathode with a high reversible capacity and good cycle life in SIBs. In layered P2-$Na_{2/3}Ni_{1/3}Mn_{2/3}O_2$, all of the Na ions can by reversibly exchanged by the Ni^{2+}/Ni^{4+} redox reaction between 2.0 and 4.5 V in SIBs, leading to a capacity of 160 mA h g^{-1} with an average discharge voltage of approximately 3.7 V versus Na^+/Na.[10] Moreover, P2-$Na_{2/3}Ni_{1/3}Mn_{2/3}O_2$ is stable in moist air, and water molecules cannot insert into the structure.[11] However, unlike in P2-$Na_{0.67}MnO_2$, which features high-spin Jahn–Teller active Mn^{3+} centers,[12] the P2–O2 phase transition occurs because of an oxygen framework shift when charging to 4.22 V in P2-$Na^+_{2/3}[Ni^{2+}_{1/3}Mn^{4+}_{2/3}]O^{2-}_2$; a large volume change is unavoidable in this region associated with the O2 phase transition. Therefore, the discharge capacity of a Na//$Na_{2/3}Ni_{1/3}Mn_{2/3}O_2$ cell fades rapidly during cycles upon charging to 4.35 V, and the available reversible capacity is limited to only 80 mA h g^{-1} in a lower potential domain of 3.8 V.[13] Recently, doping electrochemically inactive elements into transition-metal oxide layers in such systems was found to be an effective means for improving the electrochemical performance of P2-type $Na_{0.8}Li_{0.12}Ni_{0.22}Mn_{0.66}O_2$[14] and P2-type $Na_{2/3}Ni_{1/3}Mn_{2/3-x}Ti_xO_2$.[15] However, further studies are still needed to understand the phase transition mechanism and the structural changes that occur upon charge/discharge at voltages greater than 4.2 V.

Herein, considering the similar ionic radii and valence states of Mg^{2+} (0.72 Å) and Ni^{2+} (0.69 Å), a small number of nickel ions were substituted with electrochemically inactive magnesium ions to obtain Mg-substituted P2-type $Na_{0.67}Mn_{0.67}Ni_{0.33-x}Mg_xO_2$ as a novel positive electrode material for SIBs. The magnesium substitution resulted in a smoothed charge/discharge profile and improved capacity retention. Partial Mg substitution in a P2-$Na_{0.67}Mn_{0.33}Ni_{0.33}O_2$ electrode was shown to be effective in inhibiting the P2–O2 phase transition and retaining the hexagonal P2-stacked structure during cycling, which greatly enhances the structural stability of P2-$Na_{0.67}Mn_{0.67}Ni_{0.33}O_2$ and thus improves the cycling performance. Furthermore, the P2–O2 transition was

directly observed by scanning transmission electron microscopy (STEM) with atomic resolution for the first time.

A series of Mg-substituted P2-$Na_{0.67}Mn_{0.67}Ni_{0.33-x}Mg_xO_2$ ($0 \le x \le 0.33$) layered oxides were synthesized by a sol–gel method. The XRD patterns of these $Na_{0.67}Mn_{0.67}Ni_{0.33-x}Mg_xO_2$ compounds reveal that Mg doping maintained the P2 layered structure with the $P6_3/mmc$ space group (Supporting Information, Figure S1). A trace amount of a NiO impurity was also observed and is associated with the solubility limit of nickel in P2-type phases.[16] The XRD Rietveld refinement patterns presented in Figure 1 a, b suggest that the magnesium ions are located in the transition-metal oxide layer. The lattice parameters (a, c) increase upon Mg substitution owing to the difference in the ionic radii of Ni^{2+} (69 pm) and Mg^{2+} (72 pm). A summary of the crystallographic data is given in Tables S1 and S2. To study the changes in the local atom arrangement induced by oxygen shifts and Na^+ ordering upon magnesium substitution, the compound was analyzed by Raman spectroscopy (Figure S2). The three intense bands at 580, 470, and 385 cm^{-1} were attributed to the A_{1g} and E_{1g} modes of O vibrations and the E_{2g} mode of Na vibrations, respectively.[17] The E_{1g} and E_{2g} bands became more intense with an increase in Mg content, thus leading to an increase of the intensity ratio of E_{1g} and E_{2g} against A_{1g}, which indicates that the short-range structure of pristine P2-$Na_{0.67}Mn_{0.67}Ni_{0.33}O_2$ might be affected by Mg substitution. This result manifests the hypothesis that electrochemically inactive Mg^{2+} ions had been successfully incorporated into the lattice of the Mg-free material instead of forming multi-phase mixtures. P2-$Na_{0.67}Mn_{0.67}Ni_{0.33-x}Mg_xO_2$ ($x = 0.05$) powders consisted of well-formed plate-like crystals, and these plates had diameters of 1–2 μm (Figure 1 c). The morphologies of other P2-$Na_{0.67}Mn_{0.67}Ni_{0.33-x}Mg_xO_2$ ($x = 0$, 0.02, 0.10, 0.15) powders are shown in Figure S3. The lattice fringes of P2-$Na_{0.67}Mn_{0.67}Ni_{0.28}Mg_{0.05}O_2$ could be clearly observed in high resolution (HR) TEM images (Figure S4), indicating its high crystallinity. The distance of 2.51 Å between neighboring lattice fringes corresponds to the (100) planes of P2-$Na_{0.67}Mn_{0.67}Ni_{0.28}Mg_{0.05}O_2$. The energy dispersive spectroscopy (EDS) mappings for the white rectangle in Figure 1 d clearly show that sodium, manganese, nickel, magnesium, and oxygen are uniformly distributed in this particle.

The performance of various P2-$Na_{0.67}Mn_{0.67}Ni_{0.33-x}Mg_xO_2$ cathodes was examined in coin-type cells with Na metal as the counter electrode. Figure 2 a displays the galvanostatic charge/discharge curves of the first five cycles cycled at a current density of 17 mA g^{-1} (0.1 C) between 2.5 and 4.35 V. Mg-free $Na_{0.67}Mn_{0.67}Ni_{0.33}O_2$ shows a large initial discharge capacity of 143 mA h g^{-1} (0.55 Na^+) above 2.5 V and the average voltage reaches 3.7 V. However, the pristine material experiences severe capacity fading during the initial several cycles, as the length of the 4.22 V plateau is shortened on charging, which is in good agreement with a recent report by Lee et al.[13] The long plateau at 4.22 V in the charge/discharge profile of $Na_{0.67}Mn_{0.67}Ni_{0.33}O_2$ is due to the P2–O2 phase transition, which is accompanied by the gliding and expansion of the transition-metal layers, leading to the irreversible capacity loss, whereas the plateaus below 4.0 V are associated with Na^+/vacancy ordering occurring within the sodium layer.[10,13,15] It was found that a Mg content of 5 % is sufficient to smooth the charge/discharge profiles without affecting the capacity, whereas further increasing the Mg content improves the cycling

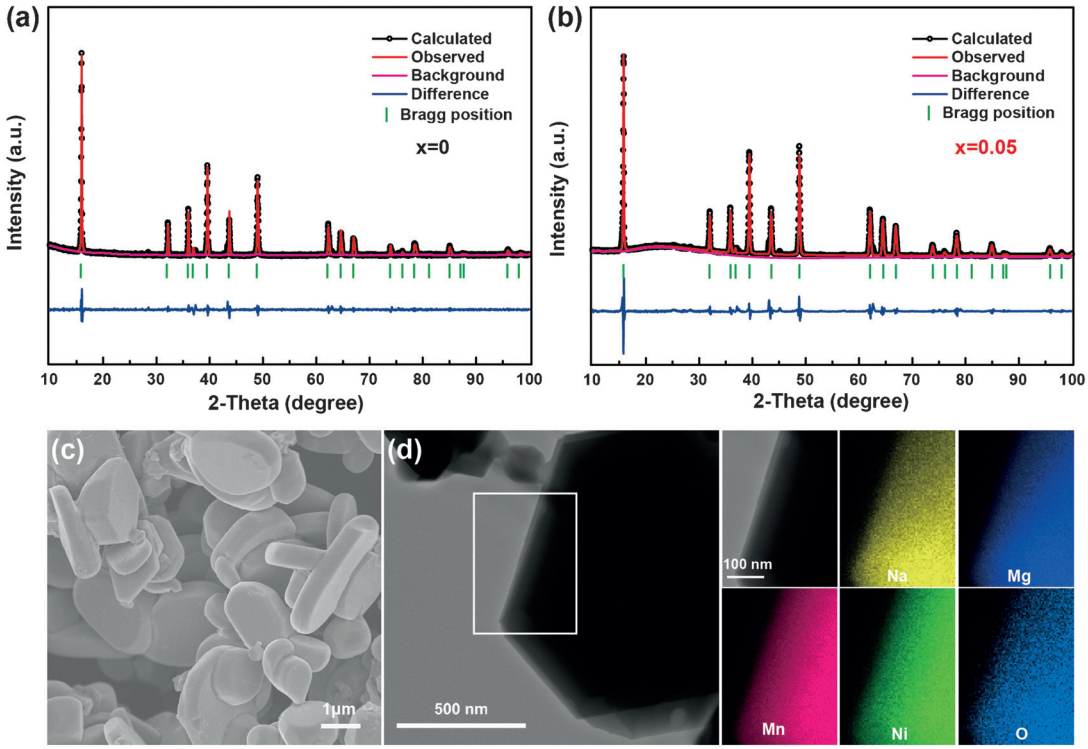

Figure 1. Rietveld refinement patterns of the powder XRD data for P2-type $Na_{0.67}Mn_{0.67}Ni_{0.33-x}Mg_xO_2$ with a) $x = 0$ and b) $x = 0.05$. c) SEM image of P2-type $Na_{0.67}Mn_{0.67}Ni_{0.33-x}Mg_xO_2$ ($x = 0.05$). d) TEM image and EDS maps of P2-type $Na_{0.67}Mn_{0.67}Ni_{0.33-x}Mg_xO_2$ ($x = 0.05$).

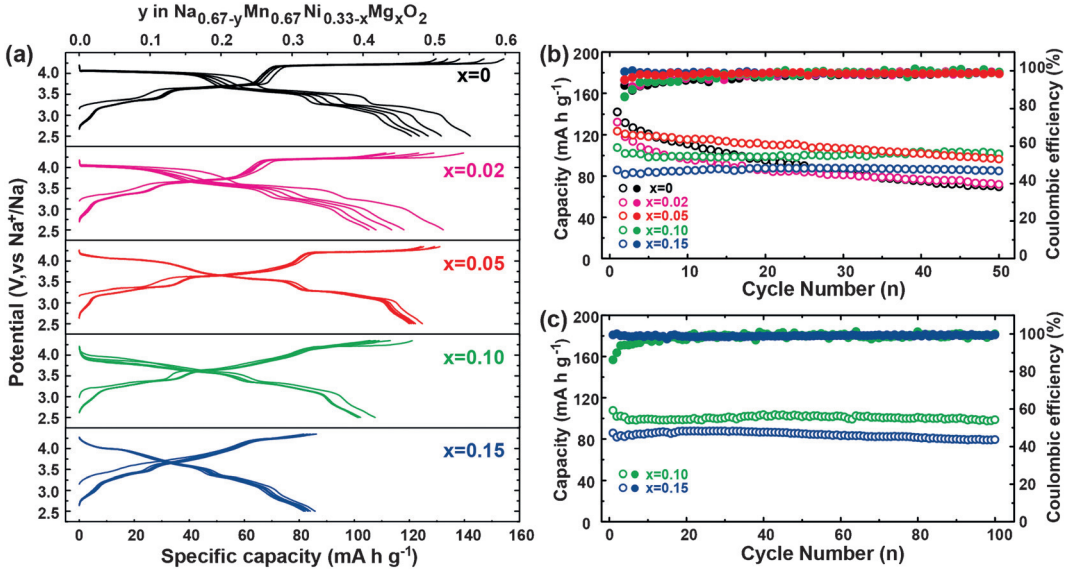

Figure 2. a) Galvanostatic charge/discharge voltage profiles of various P2-type $Na_{0.67}Mn_{0.67}Ni_{0.33-x}Mg_xO_2$ electrodes ($x=0$, 0.02, 0.05, 0.10, and 0.15) at 0.1 C (1 C = 173 mA h g^{-1}). b) Cycling performance of various P2-type $Na_{0.67}Mn_{0.67}Ni_{0.33-x}Mg_xO_2$ electrodes ($x=0$, 0.02, 0.05, 0.10, and 0.15) during 50 cycles. c) Cycling performance of P2-type $Na_{0.67}Mn_{0.67}Ni_{0.33-x}Mg_xO_2$ electrodes ($x=0.10$ and 0.15) during 100 cycles.

stability, but at the expense of a lower discharge capacity (Figure 2b). It is worth noting that the P2-$Na_{0.67}Mn_{0.67}Ni_{0.28}Mg_{0.05}O_2$ cathode delivers a reversible capacity of 123 mA h g^{-1} (0.48 Na^+) with an average discharge voltage of about 3.7 V for the initial cycles. The estimated energy density of the cathode is 455 Wh kg^{-1} with the Na metal anode (Table S3), and approximately 85% of the reversible capacity was retained after 50 cycles. The Coulombic efficiency for these electrodes with different Mg content was always greater than 98% during continuous cycle tests (Figure 2b). The long-term cycling stability of this material with a higher Mg content is excellent at current rates of 0.1 C (with capacity retentions of 91.7% for the P2-type $Na_{0.67}Mn_{0.67}Ni_{0.23}Mg_{0.10}O_2$ electrode and 92.4% for the P2-type $Na_{0.67}Mn_{0.67}Ni_{0.18}Mg_{0.15}O_2$ electrode after the 100th cycle; Figure 2c). Furthermore, the charge/discharge curves became smooth in regions below 4.0 V, and the 4.22 V plateau in the charge curves was better retained and becomes more sloping with an increase in Mg content (Figure 2a), indicating that the substitution of Ni by Mg effectively suppresses the Na^+/vacancy ordering and the gliding of the transition-metal layers.[18] This systematic variation in the charge/discharge profiles is an additional piece of evidence for the formation of Mg-substituted polycrystalline oxides instead of multi-phase mixtures.

In situ and ex situ XPS studies (Figures S5 and S6) helped with the interpretation of the status of the solid-state electrode reaction during the charge/discharge process. On charging, the Ni $2p_{3/2}$ peak changed from divalent (854.9 eV) to tetravalent (856.3 eV). When discharged to 2.5 V, the Ni $2p_{3/2}$ binding energy moves back to almost the original position while no shift is observed for Mn $2p_{3/2}$ (642.0 eV),[19] which is consistent with a previous report.[13] It indicates that within the explored 2.5–4.35 V potential window, the measured capacity for the electrodes originates from the $Ni^{2+}\leftrightarrow Ni^{4+}$ redox couple, which is identical to the cyclic voltammetry results (Figure S7). The three pairs of reversible oxidation/reduction peaks at 3.5/3.2 V, 3.8/3.5 V, and 4.3/4.0 V were ascribed to the sequential oxidation of Ni^{2+} to Ni^{3+} and Ni^{4+}, respectively. The Mg-substituted sample also showed a much better rate capability than pristine P2-type $Na_{0.67}Mn_{0.67}Ni_{0.33}O_2$ (Figure S8); however, the capacity was reduced by more than 50% at 2 C (340 mA g^{-1}) with a 2.5 V cutoff. To reduce the ohmic resistance for improving the rate capability, the electrode design needs to be further investigated with P2-type $Na_{0.67}Mn_{0.67}Ni_{0.33-x}Mg_xO_2$ as the cathode materials for SIBs.

To gain more insight into the Na intercalation/deintercalation mechanism and more specifically on the effect of the Mg substitution on the Na-driven crystal structure transformations, the material was analyzed by ex situ XRD at various charge and discharge states during the first cycle (Figure 3a–c). A detailed analysis of the ex situ XRD patterns shows that when the electrode crosses the long plateau at 4.22 V, the phase transition from hexagonal P2 to the O2 phase occurs upon Na ion extraction for Mg-free samples (Figure 3a). The original (004), (100), (012), (104), and (106) peaks that were due to the P2 phase disappear, and a new set of O2-characteristic Bragg peaks is observed (Figure 3a). For example, the new (002) peak, referred to as (002′), is located at about 21°, and the (112′) peak is found at approximately 70°. The new O2-characteristic peaks gradually become more intense as the scan number increases while the original P2 peaks weaken, showing that at this point, two phases coexist in the electrode.[10] In contrast, all of the major reflections corresponding to the P2 phase were clearly maintained for a sample with a Mg content of 5% (Figure 3b), which demonstrates that no significant phase transitions had occurred at 4.22 V. The ex situ XRD patterns (Figure S9) of all Mg-substituted electrodes charged at 4.22 V further demonstrate that the P2–O2 transition can be suppressed when $x \geq 0.05$. As further Na ions are extracted from the P2 structure of $Na_{0.67}Mn_{0.67}Ni_{0.28}Mg_{0.05}O_2$, the major reflections corresponding to the P2 phase are clearly main-

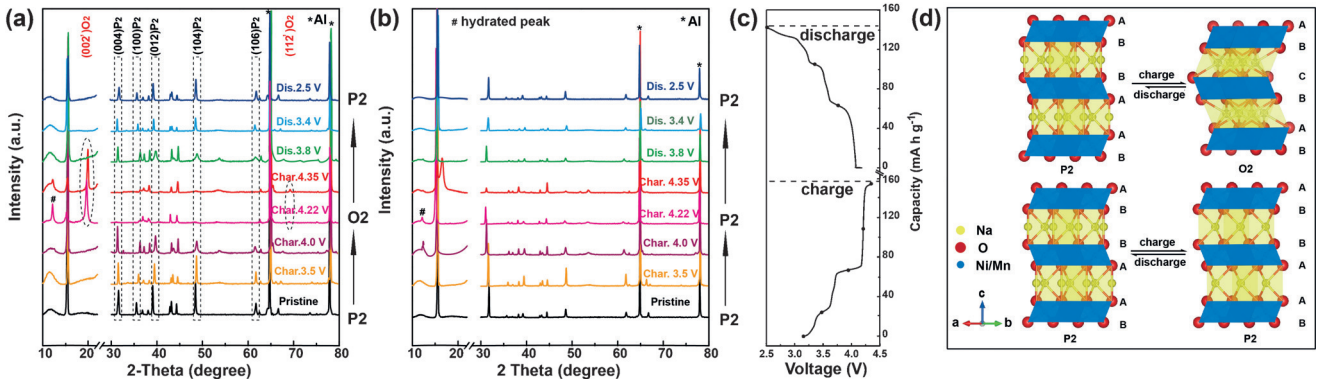

Figure 3. Ex situ XRD patterns of P2-type $Na_{0.67}Mn_{0.67}Ni_{0.33-x}Mg_xO_2$ electrodes with a) $x=0$, b) $x=0.05$ at various discharge and charge states. c) Charge/discharge profiles of P2-type $Na_{0.67}Mn_{0.67}Ni_{0.33}O_2$ electrodes; the dots indicate the depth of the charge/discharge at which the samples were taken for the ex situ XRD analysis. d) Illustration of the structural variations in Mg-free (top) and Mg-substituted (bottom) samples upon Na^+ extraction and insertion.

tained except for the (002) diffraction peak, which splits into two peaks at 4.35 V, indicating the formation of a P2 phase in a highly desodiated state with many Na vacancies.[20] Therefore, the P2–O2 phase transition is suppressed in the $Na_{0.67}Mn_{0.67}Ni_{0.28}Mg_{0.05}O_2$ electrode, which explains the smoothened charge/discharge profile and the better capacity retention upon magnesium substitution.

The illustration in Figure 3d (top) shows a complete P2–O2 phase transition based on the gliding of the TMO_2 layer as suggested by Delmas and co-workers.[21] There are two different prismatic Na sites in the pristine P2 structure, which are face-sharing with MO_6 (Na_f) and edge-sharing (Na_e). Upon charging, the Na ions in the Na_e sites are extracted faster than the Na ions in the Na_f sites owing to the higher in-plane Na^+–Na^+ electrostatic repulsion for the Na_e sites. The large prismatic sites in the P2-type phase are energetically stabilized by the large Na ions, and the TMO_2 slabs move (glide) to form octahedral sites after extraction of the Na ions in the Mg-free electrodes. This TMO_2 gliding leads to the formation of a new O2-type phase with stacking faults and a unique oxygen packing, "ABCBAB". This phase contains two crystallographically different TMO_2 layers with AB and CB oxygen arrangements. The vacancies left in between the AB and CB layers are octahedral sites.[10,22] On the other hand, the presence of immobile Mg^{2+} in the TM layers allows more Na^+ ions to reside in the prismatic sites, stabilizing the overall charge balance of the compound. Consequently, more Na ions remain in the compound upon charging, and the P2 structure is retained in the high-voltage region, which is consistent with the reduced reversible discharge capacity with an increase in Mg content.

Furthermore, apart from the variations in the intensities of some diffraction peaks during charge/discharge, some of the shifts in the peak positions are mainly due to lattice distortions induced by Na^+ extraction.[23] After one cycle, the layered P2 structure of both electrodes was completely recovered, as confirmed by the presence of sharp, well-defined XRD peaks at the original positions. The reason for this is the alignment of the TM ions along the *c* axis of the P2 structure to form trigonal-prismatic Na sites. Hence, when Na ions are reinserted back into the structure, stacking faults are eliminated in such a way that Na-ion prismatic sites can be reconstructed for the first few cycles.[13] We also compared the structural stability of the Mg-free electrode with the Mg-substituted sample after many cycles (Figure S10). The structure of the Mg-substituted electrode was well preserved even after 100 cycles, suggesting that the electrochemical reactions in the Mg-substituted samples are highly reversible, which contributes to the impressive cycling stability.

The P2–O2 phase transition was further analyzed with atomic resolution by annular bright field (ABF) and high-angle annular dark field (HAADF) STEM. Representative ABF-STEM and HAADF-STEM images of the P2- and O2-type phases of the Mg-free electrode are shown in Figure 4a and 4b, respectively, and indicate the coexistence of both faces across the 4.22 V plateau. The dark-dot contrast in the ABF-STEM images (Figure 4a) and the bright-dot contrast in the HAADF-STEM images (Figure 4b) reveal the TM (Mn, Ni) atom column positions. The dark-dot contrasts with the interlayer positions in the ABF-STEM images (Figure 4a) correspond to

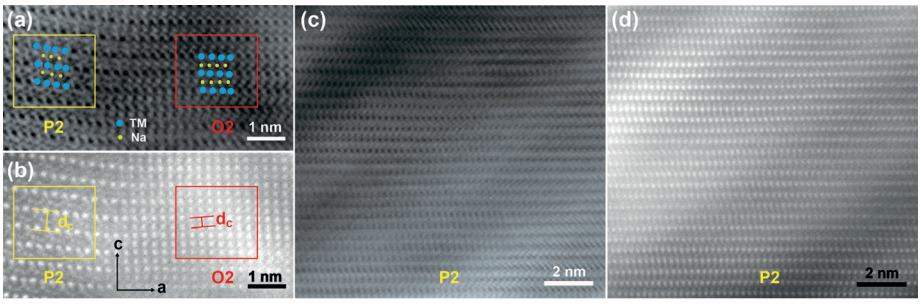

Figure 4. a) ABF- and b) HAADF-STEM images of a P2-type $Na_{0.67}Mn_{0.67}Ni_{0.33-x}Mg_xO_2$ ($x=0$) electrode when charging to 4.22 V at the [010] zone axis; the yellow and red rectangles indicate areas with the P2 and O2 structure. c) ABF- and d) HAADF-STEM images of a P2-type $Na_{0.67}Mn_{0.67}Ni_{0.33-x}Mg_xO_2$ ($x=0.05$) electrode when charging to 4.22 V.

the sodium and oxygen atom column positions in these layered structures. As shown in Figure 4a, b, the yellow and red frames reveal the detailed atomic arrangements for different P2 and O2 stacks, respectively, and these two structures are shown for comparison. The ABF-STEM observation of octahedral TMO_2 (TM = Mn/Ni) is highly consistent with the structural model. The alkali metal atoms are held in their positions by the layered TMO_2. In particular, head-to-head stacking was observed, and every two layers of TMO_2 are structurally mirror-symmetric in the P2 phase, which is distinctly different to the layer distance of each O column in the O2 phase. The coexistence of the two phases in the plateau region was also confirmed by HAADF-STEM (Figure 4b). Moreover, as a sample with the O2 phase has stacking faults, a clear decrease of the adjacent layer distance d_c from the P2 phase to the O2 phase was also observed. In contrast, ABF-STEM and HAADF-STEM images of the Mg-substituted electrode only show the P2 phase (Figure 4c, d), which is highly consistent with the ex situ XRD data. In short, the coexistence of the P2 and O2 phases was clearly characterized from the macro- to the microscale by ex situ XRD and STEM. Above all, only a few studies on the P2–O2 phase transition in Na cells have been reported thus far, and this transition has mainly been characterized by XRD analysis on the macroscale.[21,24] The phase transition was thus confirmed with atomic resolution for the first time, and this atomic-scale integration engineering should enable the modulation of the physical and chemical properties of layered oxides.

In summary, we have prepared a series of magnesium-substituted layered P2-type $Na_{0.67}Mn_{0.67}Ni_{0.33-x}Mg_xO_2$ ($0 \le x \le 0.33$) compounds as cathode materials for SIBs. The as-obtained Mg-substituted P2-$Na_{0.67}Mn_{0.67}Ni_{0.28}Mg_{0.05}O_2$ cathode delivers a reversible capacity of 123 mA h g^{-1} with an average discharge voltage of approximately 3.7 V versus Na^+/Na, leading to a high-energy density cathode material with 455 Wh kg^{-1}. The inactive Mg^{2+} ions in the TM layers allow more Na^+ ions to reside in the prismatic sites upon charging, stabilizing the overall charge balance of the compound. The P2–O2 phase transition and the Na^+/vacancy ordering in $Na_{0.67}Mn_{0.67}Ni_{0.33}O_2$ are both effectively inhibited during charging and discharging upon magnesium substitution, suggesting that the whole process involves a simple single-phase reaction with a reduced volume change, thus improving the cycling performance. Therefore, substitution with a moderate amount of inactive metals ions (such as Mg^{2+}, Zn^{2+}, Cu^{2+}, Ti^{4+}, etc.) with similar ionic radii and valence states in the transition-metal oxide layer might be an effective strategy to improve the cycling performance of P2-type compounds owing to the enhancement of the structural stability, and also gives new insight into the rational design of high-capacity and high-stability cathode materials for sodium-ion batteries.

Acknowledgements

This work was supported by the National Natural Science Foundation of China (51225204, 21303222, and 21127901), the National Key Project on Basic Research (2012CB932900), and the Chinese Academy of Sciences (CAS).

Keywords: cyclability · electrochemistry · magnesium · phase transitions · sodium-ion batteries

How to cite: *Angew. Chem. Int. Ed.* **2016**, *55*, 7445–7449
Angew. Chem. **2016**, *128*, 7571–7575

[1] a) D. Kundu, E. Talaie, V. Duffort, L. F. Nazar, *Angew. Chem. Int. Ed.* **2015**, *54*, 3431–3448; *Angew. Chem.* **2015**, *127*, 3495–3513; b) X. Deng, X. R. Liu, H. J. Yan, D. Wang, L. J. Wan, *Sci. China Chem.* **2014**, *57*, 178–183.
[2] a) I. Hasa, D. Buchholz, S. Passerini, J. Hassoun, *ACS Appl. Mater. Interfaces* **2015**, *7*, 5206–5212; b) S. Guo, P. Liu, H. Yu, Y. Zhu, M. Chen, M. Ishida, H. Zhou, *Angew. Chem. Int. Ed.* **2015**, *54*, 5894–5899; *Angew. Chem.* **2015**, *127*, 5992–5997.
[3] a) M. Peng, B. Li, H. Yan, D. Zhang, X. Wang, D. Xia, G. Guo, *Angew. Chem. Int. Ed.* **2015**, *54*, 6452–6456; *Angew. Chem.* **2015**, *127*, 6552–6556; b) Y. Qi, L. Mu, J. Zhao, Y.-S. Hu, H. Liu, S. Dai, *Angew. Chem. Int. Ed.* **2015**, *54*, 9911–9916; *Angew. Chem.* **2015**, *127*, 10049–10054.
[4] a) Y. You, X.-L. Wu, Y.-X. Yin, Y.-G. Guo, *Energy Environ. Sci.* **2014**, *7*, 1643; b) Y. You, X. Yu, Y. Yin, K.-W. Nam, Y.-G. Guo, *Nano Res.* **2014**, *8*, 117–128.
[5] C. Delmas, C. Fouassier, P. Hagenmuller, *Physica B* **1980**, *99*, 81–85.
[6] C. Delmas, J.-J. Braconnier, C. Fouassier, P. Hagenmuller, *Solid State Ionics* **1981**, *3–4*, 165–169.
[7] X. Ma, H. Chen, G. Ceder, *J. Electrochem. Soc.* **2011**, *158*, A1307.
[8] S. Komaba, N. Yabuuchi, T. Nakayama, A. Ogata, T. Ishikawa, I. Nakai, *Inorg. Chem.* **2012**, *51*, 6211–6220.
[9] I. Hasa, D. Buchholz, S. Passerini, B. Scrosati, J. Hassoun, *Adv. Energy Mater.* **2014**, *4*, 1400083.
[10] Z. Lu, J. R. Dahn, *J. Electrochem. Soc.* **2001**, *148*, A1225.
[11] Z. Lu, J. R. Dahn, *Chem. Mater.* **2001**, *13*, 1252–1257.
[12] K. Hemalatha, M. Jayakumar, P. Bera, A. S. Prakash, *J. Mater. Chem. A* **2015**, *3*, 20908–20912.
[13] D. H. Lee, J. Xu, Y. S. Meng, *Phys. Chem. Chem. Phys.* **2013**, *15*, 3304–3312.
[14] J. Xu, D. H. Lee, R. J. Clément, X. Yu, M. Leskes, A. J. Pell, G. Pintacuda, X.-Q. Yang, C. P. Grey, Y. S. Meng, *Chem. Mater.* **2014**, *26*, 1260–1269.
[15] H. Yoshida, N. Yabuuchi, K. Kubota, I. Ikeuchi, A. Garsuch, M. Schulz-Dobrick, S. Komaba, *Chem. Commun.* **2014**, *50*, 3677–3680.
[16] J. M. Paulsen, J. R. Dahn, *Solid State Ionics* **1999**, *126*, 3–24.
[17] J. F. Qu, W. Wang, Y. Chen, G. Li, X. G. Li, *Phys. Rev. B* **2006**, *73*, 092518.
[18] Y. Wang, R. Xiao, Y. S. Hu, M. Avdeev, L. Chen, *Nat. Commun.* **2015**, *6*, 6954.
[19] Y. M. Wang, Y. J. Wang, F. Wang, *Nanoscale Res. Lett.* **2014**, *9*, 197.
[20] E. Talaie, V. Duffort, H. L. Smith, B. Fultz, L. F. Nazar, *Energy Environ. Sci.* **2015**, *8*, 2512–2523.
[21] C. Delmas, J.-J. Braconnier, P. Hagenmuller, *Mater. Res. Bull.* **1982**, *17*, 117–123.
[22] Z. Lu, J. R. Dahn, *J. Electrochem. Soc.* **2001**, *148*, A710.
[23] D. Carlier, J. H. Cheng, R. Berthelot, M. Guignard, M. Yoncheva, R. Stoyanova, B. J. Hwang, C. Delmas, *Dalton Trans.* **2011**, *40*, 9306–9312.
[24] a) J. M. Paulsen, J. R. Dahn, *J. Electrochem. Soc.* **2000**, *147*, 2478–2485; b) J. M. Paulsen, R. A. Donaberger, J. R. Dahn, *Chem. Mater.* **2000**, *12*, 2257–2267; c) D. Carlier, I. Saadoune, L. Croguennec, M. Menetrier, E. Suard, C. Delmas, *Solid State Ionics* **2001**, *144*, 263–276.

Received: March 3, 2016
Revised: March 24, 2016
Published online: May 3, 2016

